Monatshefte für Chemie 136, 1139–1155 (2005)
DOI 10.1007/s00706-004-0257-8

Monatshefte für Chemie
Chemical Monthly
Printed in Austria

Preparation and Characterization of Sulfadiazine *Schiff* Base Complexes of Co(II), Ni(II), Cu(II), and Mn(II)

Kamal Y. El-Baradie*

Chemistry Department, Faculty of Science, Tanta University, Tanta, Egypt

Received August 16, 2004; accepted (revised) September 15, 2004
Published online March 18, 2005

Summary. Complexes of Co(II), Ni(II), Cu(II), and Mn(II) containing *Schiff* base NOS donor ligands have been synthesised *via* chemical and electrochemical techniques. The structure of the complexes has been elucidated by elemental analysis, conductance, magnetic susceptibility measurements, IR, ESR, electronic spectral studies and thermal techniques (TGA and DTA). The electrochemical behaviour of the metal complexes was studied using DC polarography and cyclic voltammetry. Antimicrobial activity of the title *Schiff* base and its complexes has been tested against different microorganisms.

Keywords. Sulfadiazine; *Schiff* base; Complexes, Co(II), Ni(II), Cu(II), Mn(II); Biological activity.

Introduction

Schiff bases have played an important role in the development of coordination chemistry as they readily form stable complexes with most transition metals. *Schiff* bases and their metal complexes are becoming increasingly important as biochemical [1], analytical [2, 3], industrial [4] reagents and redox catalysts [5–8] as well as pigment dyes [9, 10]. What appears more important, is that *Schiff* bases and their metal complexes are useful in biological and pharmaceutical applications [11–13]. In recent years, there has been considerable interest in the chemistry of sulfadrugs and their metal complexes [14, 15]. However, the literature on the chemistry of *Schiff* base complexes derived from sulfadrugs, especially their structure characteristics, is rather incomplete.

Schiff bases and its metal complexes display obvious inhibitor effects against *Gram* positive bacteria (*Staphylococcus aureus* and *Bacillus subtilis*) and *Gram* negative bacteria (*Escherichia coli* and *Pseudomonos aeruginosa*). These studies reported the minimum inhibitor concentration of the used *Schiff* base and its metal complexes on these microorganism [16].

* E-mail: kyelbaradie@hotmail.com

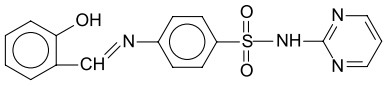

Fig. 1. Structure of *Schiff* base

The present paper deals with the chemical and electrochemical synthesis and structural studies of Co(II), Ni(II), Cu(II), and Mn(II) complexes with a *Schiff* base derived from sulfadiazine and salicylaldehyde (Fig. 1).

Results and Discussion

The analytical and physical data of the metal complexes are represented in Table 1. The complexes are air stable for a long time, insoluble in different organic solvents but soluble in *DMF*. The analytical data of the metal complexes indicate that the complexes have 2:1 and 1:2 metal-ligand stoichiometry for chemical and electrochemical methods of preparation, respectively. The values of the molar conductance ($10^{-3}\,M$ solutions in *DMF*) are in the range 10.1–19.3 $\Omega^{-1}\,cm^2\,mol^{-1}$

Table 1. Analytical and physical data of *Schiff* base complexes

No.	Formula of complex (mol. wt)	$\frac{\Lambda}{\Omega^{-1}\,cm^2 mol^{-1}}$	$\frac{\mu_{eff}}{BM}$	g_{eff} (ESR)
1	$[CoL_2(H_2O)_2]H_2O$ $C_{34}H_{32}N_8O_9S_2Co$ (818.93)	10.9	5.1	2.0165
2	$[Co_2L(AcO)_2(H_2O)_4]3H_2O$ $C_{21}H_{32}N_4O_{14}SCo_2$ (713.86)	19.3	4.9	2.0062
3	$[NiL_2(H_2O)_2]H_2O$ $C_{34}H_{32}N_8O_9S_2Ni$ (818.7)	9.9	3.1	–
4	$[Ni_2L(AcO)_2(H_2O)_4]2H_2O$ $C_{21}H_{30}N_4O_{13}SNi_2$ (695.4)	18.9	2.95	–
5	$[CuL_2]2H_2O$ $C_{34}H_{30}N_8O_8S_2Cu$ (805.54)	10.1	1.82	2.1587
6	$[Cu_2L(AcO)_2(H_2O)_2]2H_2O$ $C_{21}H_{26}N_4O_{11}SCu_2$ (669.08)	17.9	1.79	2.0086
7	$[MnL_2(H_2O)_2]2H_2O$ $C_{34}H_{34}N_8O_{10}S_2Mn$ (832.93)	12.5	5.56	2.0123
8	$[Mn_2L(AcO)_2(H_2O)_4]2H_2O$ $C_{21}H_{30}N_4O_{13}SMn_2$ (687.86)	16.4	4.92	2.0072

Table 2. Results of thermogravimetric analysis of mononuclear Co(II) and Mn(II) complexes

Comp. no	Complex (mol. wt)	Process	Temp. range/°C	Mass loss/%	
				Found	Calc.
1	$[CoL_2(H_2O)_2]H_2O$ (818.93)	a) Loss of lattice water molecule	30–105	2.5	2.2
	$[CoL_2(H_2O)_2]$ (800.93)	b) Loss of coordinated water	105–255	4.6	4.4
	$[CoL_2]$ (764.93)	c) Loss of 2-imino-pyrimidine	255–390	23.6	23.2
	$[CoL_2]$ (574.93)	d) Loss of $2SO_2 + 2$ benzene rings	390–585	34.3	34.6
	Degradation of whole molecule and formation of CoO as a final product (585–760°C)				
7	$[MnL_2(H_2O)_2]2H_2O$ (832.93)	a) Loss of lattice water molecules	30–115	4.1	4.3
	$[MnL_2(H_2O)_2]$ (796.93)	b) Loss of coordinated water	115–230	4.4	4.3
	$[MnL_2]$ (760.93)	c) Loss of 2-imino-pyrimidine	230–410	21.9	22.8
	$[MnL_2]$ 570.93	d) Loss of $2SO_2 + 2$ benzene rings	410–565	34.5	34.1
	Degradation of whole molecule and formation of MnO_2 as a final product (565–785°C)				

indicating a non-electrolytic nature of these complexes [17]. This reveals the involvement of the acetate ion in the coordination sphere of the metal ions in the binuclear complexes **2**, **4**, **6**, and **8**. The mononuclear complexes **1**, **3**, **5**, and **7** are deprived of anions.

Thermal Analysis

The results of thermogravimetric analysis of mononuclear and binuclear Co(II) and Mn(II) complexes **1**, **2**, **7**, and **8** are collected in Tables 2 and 3.

The thermograms of mononuclear Co(II) and Mn(II) complexes **1** and **7** show that the weight losses in temperature ranges 30–105 and 30–115°C are attributed to removal of one and two lattice water molecules associated with endothermic peaks at 72 and 95°C in the DTA thermogram for complexes **1** and **7**, respectively. The weight losses in the temperature ranges at 105–255 and 115–230°C are attributed to the elimination of the two coordinated water molecules with endothermic peaks at 139 and 176°C for both complexes. The removal of 2-iminopyrimidine takes place within the temperature ranges 255–390 and 230–410°C with exothermic peaks at 352 and 372°C in the DTA thermogram followed by loss of two SO_2 molecules and two benzene rings within the temperature ranges 390–585 and 410–565°C associated with exothermic peaks at 557 and 532°C for complexes **1** and **7**, respectively. The decomposition steps within the temperature ranges 585–760 and 565–785°C

Table 3. Results of thermogravimetric analysis of binuclear Co(II) and Mn(II) complexes

Comp. no	Complex (mol. wt)	Process	Temp. range/°C	Mass loss/%	
				Found	Calc.
2	$[Co_2L(AcO)_2(H_2O)_4]3H_2O$ (713.86)	a) Loss of lattice water molecule	30–130	7.7	7.6
	$[Co_2L(AcO)_2(H_2O)_4]$ (659.86)	b) Loss of coordinated water	130–240	9.8	10.0
	$[CoL(AcO)_2]$ (587.85)	c) Loss of 2 acetic acid	240–430	17.4	16.8
	[CoL] (467.86)	d) Loss of benzene ring	430–590	10.8	10.6
	Degradation of whole molecule and formation of Co_2O_3 as a final product (590–765°C)				
8	$[Mn_2L(AcO)_2(H_2O)_4]2H_2O$ (687.86)	a) Loss of lattice water molecules	30–120	5.2	5.2
	$[Mn_2L(AcO)_2(H_2O)_4]$ (655.86)	b) Loss of coordinated water	120–265	10.3	10.5
	$[Mn_2L(AcO)_2]$ (583.86)	c) Loss of 2 acetic acid	265–455	17.1	17.4
	$[Mn_2L]$ (463.86)	d) Loss of benzene ring	455–610	11.6	11.3
	Degradation of whole molecule and formation of MnO_2 as a final product (610–790°C)				

with broad exothermic peaks at 628 and 642°C are due to decomposition of the remainder ligand molecule leading to CoO and MnO_2 as final products.

The binuclear Co(II) and Mn(II) complexes **2** and **8** were thermally decomposed in several steps supported by DTA data. The thermograms of complexes **2** and **8** show that the three lattice water molecules for complex **2** and two lattice water molecules for complex **8** are eliminated at the temperature ranges 30–130 and 30–120°C with endothermic peaks at 77 and 97°C. The four coordinated water molecules are eliminated for both complexes **2** and **8** within the temperature ranges 130–240 and 120–265°C with endothermic peaks at 180 and 198°C for complexes **2** and **8**. The losses in weight within the temperature ranges 240–430 and 265–455°C are due to removal of two acetate groups with strong exothermic peaks at 400 and 392°C for complexes **2** and **8**. The decrease in weight in the temperature ranges 430–590 and 455–610°C are due to the elimination of a benzene ring. This step is confirmed by strong exothermic peaks at 575 and 560°C for complexes **2** and **8**, respectively. The last step of decomposition lies within the temperature ranges 590–765 and 610–790°C associated with broad exothermic peaks at 615 and 645°C, corresponding to the decomposition of the ligand leading to Co_2O_3 and MnO_2 for complexes **2** and **8**.

The order, n and activation energy, E^*, of the decomposition steps were determined using the *Coats-Redfern* equation [18] as given in Eqs. (1) and (2).

$$\ln\left[\frac{1-(1-\alpha)^{1-n}}{(1-n)T^2}\right] = M/T + B \quad \text{for } n \neq 1 \tag{1}$$

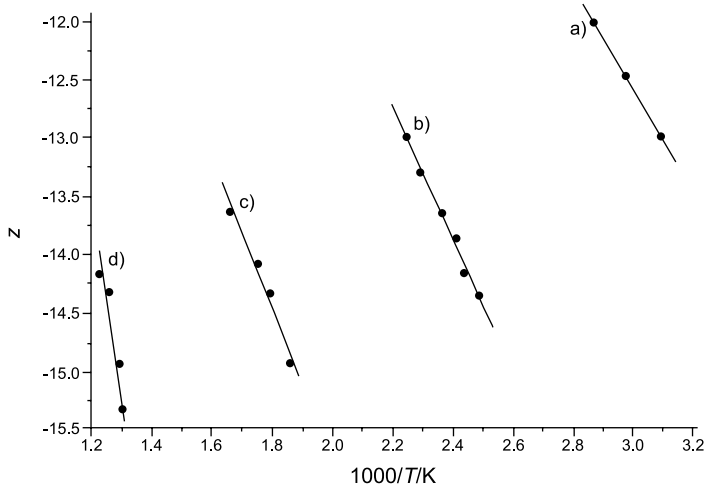

Fig. 2. *Coats-Redfern* plots for complex 1

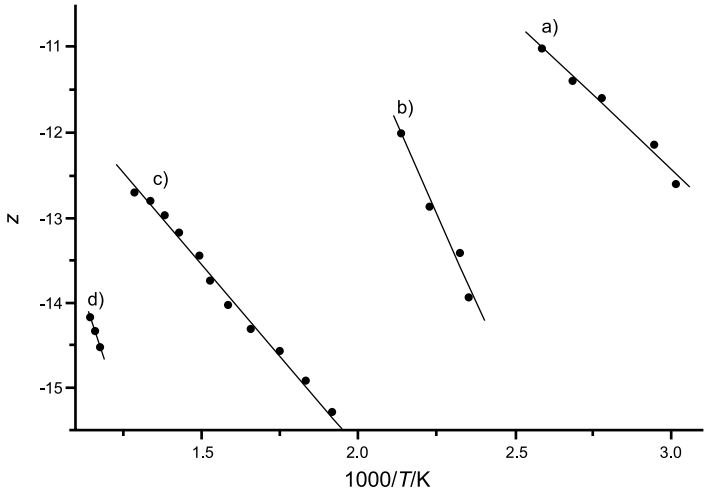

Fig. 3. *Coats-Redfern* plots for complex **2**

$$\ln\left[\frac{-\ln(1-\alpha)}{T^2}\right] = M/T + B \quad \text{for } n = 1 \tag{2}$$

Where $M = -E^*/R$ and $B = \ln AR/\Phi E^*$ and E^*, R, A, and Φ are the activation energy, gas constant, pre-exponential factor, and heating rate, respectively.

The correlation coefficient, r, is calculated using the least squares method for different values of n. The value of $\ln[(1-(1-\alpha)^{1-n})/(1-n)T^2]$ or $\ln[-\ln(1-\alpha)/T^2]$ from *Coats-Redfern* equation is plotted against $1000/T$ (see Figs. 2 and 3). From the intercept and slope of such linear stage, the A and E^* values were determined, respectively. The other kinetic parameters (ΔH^*, ΔS^*, and ΔG^*) were calculated using the relationships given in Eqs. (3)–(5).

$$\Delta H^* = E^* - RT \tag{3}$$

Table 4. Values of correlation coefficient, slope, and intercept of the thermal decomposition and activation parameters of complex **1**

Step	*Coats-Redfern* equation				$\frac{T}{\mathrm{K}}$	$\frac{E^*}{\mathrm{kJ\,mol^{-1}}}$	$\frac{\Delta H^*}{\mathrm{kJ\,mol^{-1}}}$	$\frac{A}{\mathrm{kJ\,mol^{-1}}}$	$\frac{\Delta S^*}{\mathrm{kJ\,K^{-1}\,mol^{-1}}}$	$\frac{\Delta G^*}{\mathrm{kJ\,mol^{-1}}}$
	n	*r*	Slope	Intercept						
	0	0.9962	−3.6585	−2.0828						
1	0.5	0.9956	−4.4210	0.2704	345	44.1	41.27	20529.1	−0.164	97.85
	1	0.9923	−5.3112	3.0072						
	0	0.9915	−5.6126	−2.4722						
2	0.5	0.9924	−4.9691	−0.9739	412	36.7	33.27	73.7	−0.212	120.5
	1	0.9934	−4.4144	0.64755						
	0	0.9985	−4.8198	−5.3121						
3	0.5	0.9986	−5.2971	−4.3703	625	42.6	37.45	10.3	−0.232	182.2
	1	0.9987	−5.8048	−3.3709						
	0	0.9937	−3.0523	−10.2139						
4	0.5	0.9952	−3.6245	−9.3451	830	35.3	28.38	3.86	−0.242	229.4
	1	0.9962	−4.2462	−8.4054						

Table 5. Values of correlation coefficient, slope and intercept of the thermal decomposition and activation parameters of complex **2**

Step	*Coats-Redfern* equation				$\frac{T}{\mathrm{K}}$	$\frac{E^*}{\mathrm{kJ\,mol^{-1}}}$	$\frac{\Delta H^*}{\mathrm{kJ\,mol^{-1}}}$	$\frac{A}{\mathrm{kJ\,mol^{-1}}}$	$\frac{\Delta S^*}{\mathrm{kJ\,K^{-1}\,mol^{-1}}}$	$\frac{\Delta G^*}{\mathrm{kJ\,mol^{-1}}}$
	n	*r*	Slope	Intercept						
	0	0.9542	−1.6753	−7.6151						
1	0.5	0.9817	−2.4127	−5.3116	350	27.34	25.02	65.12	−0.212	99.06
	1	0.9938	−3.3603	−2.3828						
	0	0.9909	−6.4174	1.2360						
2	0.5	0.9948	−7.7798	4.4611	453	68.79	65.01	4.3×10^5	−0.141	128.7
	1	0.9950	−9.4183	8.3275						
	0	0.9899	−3.3148	−8.8645						
3	0.5	0.9978	−4.0397	−7.5533	673	35.83	30.21	0.88	0.253	200.3
	1	0.9956	−4.9489	−5.9222						
	0	0.9974	−7.9474	−5.3265						
4	0.5	0.9983	−9.1217	−3.8583	848	86.41	79.33	212.7	−0.21	257.4
	1	0.9987	−10.392	−2.2739						

$$\Delta S^* = R[\ln(Ah/kT) - 1] \tag{4}$$

$$\Delta G^* = \Delta H^* - T\Delta S^* \tag{5}$$

Where k is *Boltzmann*'s constant and h is *Planck*'s constant. The order and kinetic parameters of complexes are listed in Tables 4 and 5. The ΔS^* values were found to be negative which indicated that the activated complex is more ordered than the reactant and/or the thermal decomposition reaction is slower than normal. ΔG^*

values increase with increasing the order of the decomposition stages which indicates that at high temperatures the ligand decomposes and require more energy for its rearrangement in the activated state.

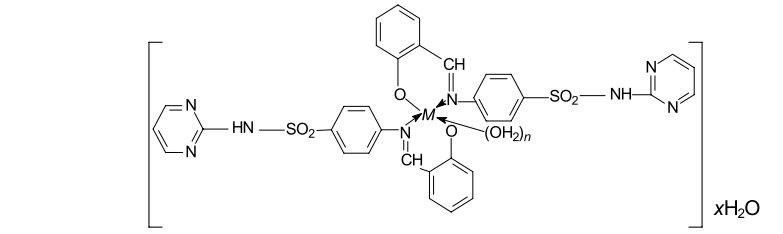

	M	*n*	*x*
1	Co(II)	2	1
7	Mn(II)	2	2

(A) loss of lattice and coordinated water molecules

30-255°C

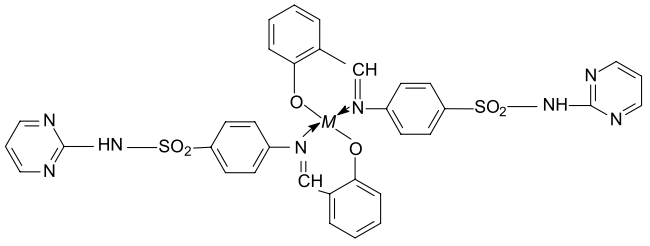

(B) loss of 2-iminopyrimidine

230-410°C

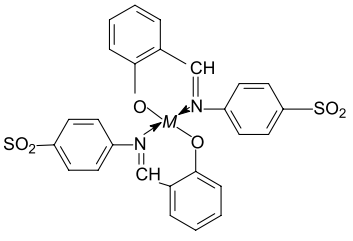

(C) loss of $2SO_2$ + 2 benzene rings

390-585°C

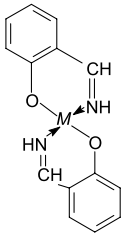

(D) decomposition of ligand

CoO for complex **1** and MnO_2 for complex **7**

565-785°C

Scheme 1

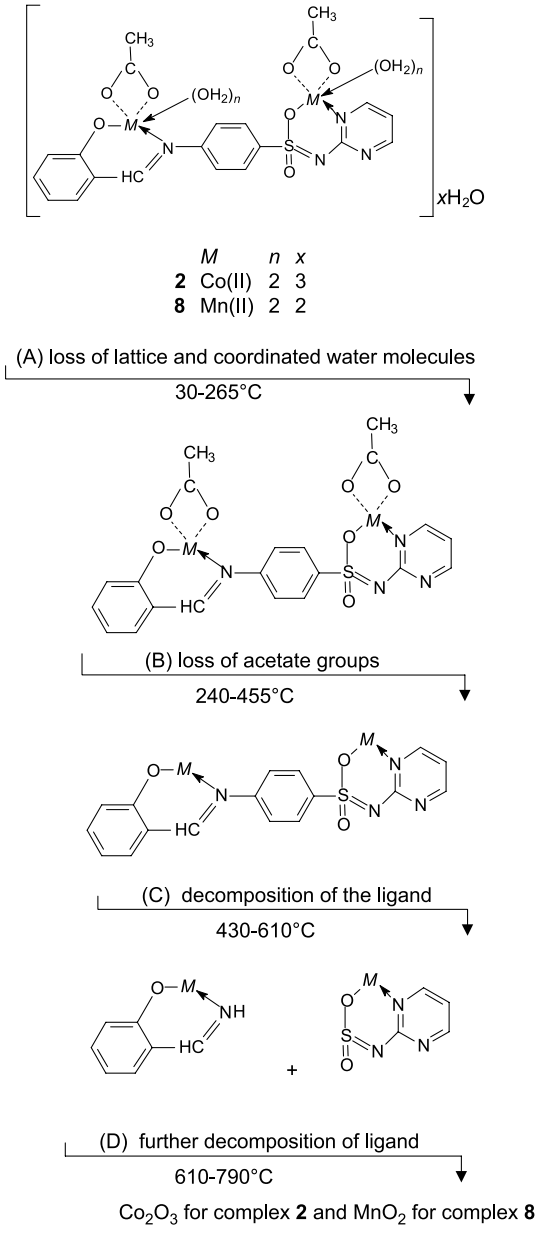

Scheme 2

Based on the data of thermal analysis, the decomposition of mononuclear and binuclear complexes can be represented as shown in Schemes 1 and 2.

IR Spectra

The most important IR assignments in the spectrum of the free *Schiff* base as well as the bonding sites have been determined by a careful comparison of the spectrum of the ligand and its metal complexes (Table 6). The IR spectrum of *Schiff* base shows broad bands at 3458 cm^{-1} (ν_{OH}) and 3100 cm^{-1} (ν_{NH}). The strong bands at

Table 6. IR and electronic spectra of complexes **1–8**

No.	IR spectra						Electronic spectra			
	ν_{OH} / cm^{-1}	$\nu_{C=N}$ / cm^{-1}	$\nu_{C=N}$ / cm^{-1}	ν_{M-N} / cm^{-1}	ν_{M-N} / cm^{-1}	ν_{M-O} / cm^{-1}	ν / cm^{-1}	D_q / cm^{-1}	B / cm^{-1}	β
1	3468	1600	1556	445	362	572	15740 18860	840	839	0.86
2	3430	1605	1583	450	377	560	17668 20790	934	897	0.92
3	3436	1581	1550	447	386	575	14700 23800	921	723	0.69
4	3360	1602	1584	467	366	572	16000 25641	1011	754	0.72
5	3433	1588	1546	445	360	579	14280 18860	–	–	–
6	3436	1607	1584	457	332	574	15385 20408	–	–	–
7	3380	1585	1550	450	365	560	15490 21277	–	–	–
8	3420	1605	1538	465	380	572	18780 23150	–	–	–

1618 and 1582 cm^{-1} are attributed to the $\nu_{C=N}$ vibration of the azomethine and pyrimidine ring. The *Schiff* base exhibits a medium intensity band at 2599 cm^{-1} which is assigned to the intramolecular H-bonding vibration (O–H–N). This situation is common for aromatic azomethine compounds containing an OH group in ortho position to a C=N group [19]. In the metal complexes, this band disappeared completely. The two bands at 1339 and 1166 cm^{-1} are assigned to the v_{asy} and v_{sym} of the SO_2 group.

The IR spectra of the binuclear metal complexes **2**, **4**, **6**, and **8** show that the *Schiff* base behaves as dibasic tetradentate ligand whereas for the mononuclear complexes **1**, **3**, **5**, and **7** the *Schiff* base is monobasic bidentate. The mode of chelation is elucidated from the following evidences:

1) The disappearance of v_{OH} bands in the complexes reveals the deprotonation of the enolic and phenolic OH groups indicating that the proton of the OH group is displaced by the metal ions on complex formation.
2) The IR spectra of complexes **2**, **4**, **6**, and **8** showed shift to lower wavenumbers in $v_{C=N}$ of both the azomethine and pyrimidine moieties by 10–30 and 26–36 cm^{-1}, respectively. These data suggest that both the azomethine and one nitrogen atom of the pyrimidine ring are involved in coordination to the metal ions. For mononuclear complexes **1**, **3**, **5**, and **7**, the $v_{C=N}$ band of the pyrimidine ring in the range 1584–1546 cm^{-1} is unaffected by complexation indicating that the N-atoms of the pyrimidine ring are not involved in complex formation.
3) For the acetate complexes, the bands due to ν_{asy} and ν_{sym} of the acetate group are observed at 1444 and 1344 cm^{-1} for Co(II) complex **2**, and at 1446 and

1386 cm^{-1} for Ni(II) complex **4**. The Δv values in cm^{-1} for complexes **2** and **4** are 100 and 60 cm^{-1} which can be taken as evidence for the existence of bidentate acetate groups [20, 21]. The Cu(II) complex **6** and Mn(II) complex **8** show two bands due to v_{asy} and v_{sym} of the acetate group at 1615 and 1386 cm^{-1}, and 1610 and 1400 cm^{-1}, respectively. The Δv values between v_{asy} and v_{sym} are 229 and 210 cm^{-1} for complexes **6** and **8**, respectively. These values are higher than 200 cm^{-1} which support the presence of monodentate acetate groups [20, 21].

4) The presence of water molecules in the complexes leads to the broad bands at 3468–3410 cm^{-1} (v_{H_2O}) and 1610–1595 cm^{-1} (δ_{H_2O}) for both lattice and coordinated water molecules. The coordinated water molecules give also bands at 940–920 cm^{-1} (ρ_{H_2O}), 874–846 cm^{-1} (ω_{H_2O}). The latter bands ($\rho_{H_2O} + \omega_{H_2O}$) are absent in the spectra of complex **5** which contains only lattice water [22]. The IR bands of the lattice water molecules are absent in the spectrum of complex **5** heated at 150°C for 2 hours, whereas that of complex **7** heated at 150°C showed an obvious decrease in the intensity of the v_{H_2O} and δ_{H_2O} bands. When complex **7** was heated to 250°C for 2 hours, bands due to the various types of vibrations of the coordinated water molecules disappeared. However it is worthy to mention that the IR spectrum in the latter case was found to suffer some alteration presumably due to the occurrence of some decomposition in the anhydrous complex.
5) A shift of the v_{S-N} band is observed in the IR spectra of the complexes, 943–935 cm^{-1}, with respect to that of the ligand, 913 cm^{-1}. This could be attributed to deprotonation of the sulfonamido group and consequently the shortening of the S–N bond distance.
6) The appearance of new bands in the region 579–560 and 386–332 cm^{-1} assignable to v_{M-O} and v_{M-N}, respectively [23], reflects the bonding of the metal ions to oxygen and nitrogen atoms.
7) The spectra of complexes **2**, **4**, **6**, and **8** do not show characteristic sulfonamide (–SO_2NH–) group frequencies [$v_{SO_2\ (asy)}$ and $v_{SO_2\ (sym)}$] and NH vibrations. This commensurates that in these complexes, the oxygen of the sulfonamide group coordinates in the enolic form through deprotonation [24]. The appearance of new bands characteristic of δ_{NSO} in the ranges 1448–1410 and 1354–1340 cm^{-1} further confirm enolisation of the *Schiff* base [25].

Magnetic Moments and Electronic Spectra

The room temperature magnetic moment (Table 1) for the Co(II) complexes **1** and **2** are 5.1 and 4.9 BM, respectively, which confirm the octahedral structure of these complexes [23].

The electronic spectra of Co(II) complexes **1** and **2** recorded as Nujol mull (Table 6) display two bands at 15740, 18860 and 17668, 20790 cm^{-1}, respectively. These bands are assigned to $^4T_{1g} \rightarrow {}^4T_{2g}$ (v_2) and $^4T_{1g} \rightarrow {}^4T_{2g}$ (p) (v_3) [26]. Also, the ligand field parameters (Table 6) are additional evidence for the octahedral structure [27].

The Ni(II) complexes **3** and **4** show magnetic moment values of 3.1 and 2.95 BM, respectively, expected for spin free octahedral Ni(II) complexes [28].

The Nujol mull electronic spectra of Ni(II) complexes **3** and **4** show two bands at 14700, 23800 and 16000, 25641 cm^{-1}, respectively, which can be assigned to the $^3A_{2g} \rightarrow {}^3T_{1g}(F)$ (v_2) and $^3A_{2g} \rightarrow {}^3T_{1g}(p)$ (v_3) transitions [26]. The calculated D_q, B, and β values lie in the range reported for an octahedral environment around a Ni(II) ion [29]. The β values obtained are less than unity suggesting considerable amount of covalent character of the metal ligand bonds. Also, the β values for the complexes are lower than the free ion's value, thereby indicating orbital overlap and delocalization of d-orbitals.

The magnetic moment values for Cu(II) complexes **5** and **6** are 1.82 and 1.79 BM. These values indicate the absence of any appreciable spin coupling between unpaired electrons belonging to different copper atoms. The electronic spectral bands appeared at 14280, 18860 and 15385, 20408 cm^{-1} for Cu(II) complexes **5** and **6**, respectively. These bands are assignable to transitions $^2B_{1g} \rightarrow {}^2A_{1g}$ and $^2B_{1g} \rightarrow {}^2E_g$ of a square planar geometry [30]. The magnetic moment values for Mn(II) complexes **7** and **8** are 5.56 and 4.92 BM, respectively which confirm the octahedral structure of these complexes. The lower value for complex **8** can be attributed to antiferromagnetic interaction between adjacent Mn(II) ions [31]. The electronic absorption spectra of Mn(II) complexes **7** and **8** display two bands at 15490, 21277 and 18780, 23150 cm^{-1}, respectively, which correspond to the octahedral configuration. These bands are assigned to $^6A_{1g} \rightarrow {}^4T_{1g}(4G)$ and $^6A_{1g} \rightarrow {}^4E_g(G)$ transitions [32].

ESR Spectra

The g_{eff} values of mononuclear and binuclear complexes under investigation were calculated and collected in Table 1.

The X-band ESR spectra of Co(II) complexes **1** and **2** at room temperature show an intense broad signal with no hyperfine structure with g_{eff} values 2.0165 and 2.0062 which are characteristic of Co(II) octahedral structure [33]. The ESR spectra of Cu(II) complexes **5** and **6** give a broad signal with no hyperfine structure with g_{eff} values 2.1587 and 2.0086 which indicate that Cu(II) complexes have square planar geometry. The ESR spectra of Mn(II) complexes **7** and **8** show broad signals with $g_{eff} = 2.0123$ and 2.0072, which suggest the existence of octahedral high spin Mn(II) complexes [34].

The more positive contribution in the g_{eff} values of the mononuclear and binuclear complexes compared to the value of a free electron, 2.0023, indicates an increase in the covalent nature of the bonding between the metal ion and the ligand molecule [35].

Electrochemical Studies

The electroreduction of the ligand and its metal complexes was studied using DC polarography at the dropping mercury electrode and cyclic voltammetry on a hanging mercury drop in a medium 0.1 *M* KCl containing 50% *v/v DMF*.

The DC polarogram of the ligand displays a single wave with $E_{1/2} = -0.17$ V *vs.* SCE representing the reduction of the azomethine group. The reduction process was found to be irreversible as gathered from the analysis of the wave using the fundamental equation [36]. The αn_a value amounted to 1.4, hence the most prob-

Table 7. Polarographic data obtained for some complexes in 0.1 *M* KCl at 25°C; values of αn_a and α were calculated from reciprocal slope (S_1) of the log (i/i_d) $-E$ plots

No.	i_d μA		$-E_{1/2}$/V		$\frac{\text{Slope}(S_1)}{\text{mV}}$		αn_a		α for $n_a = 2$	
	(a)	(b)	(a)	(b)	(a)	(b)	(a)	(b)	(a)	(b)
Ligand	2.12	0.63	0.17	1.33	42.0	14.5	1.4	4.06	0.7	2.03
Complex **1**	1.5	0.92	0.24	1.1	33.5	22.1	1.76	2.67	0.88	1.335
Complex **2**	2.75	–	0.13	–	27.4	–	2.15	–	1.075	–
Complex **3**	2.32	1.17	0.13	1.5	25.1	35.9	2.35	1.64	1.175	0.82
Complex **5**	1.97	0.4	0.33	1.2	51.7	30.1	1.14	1.96	0.57	0.98

(a) First wave; (b) second wave

able α value would be obtained for $n_a = 2$, and the rate determining step in the electrode process would involve two electrons. The total number of electrons involved in the electrode process can be calculated from the i_d value making use of the *Ilkovic* equation. The value thus determined amounts to ~3.5 μA denoting that four electrons are consumed in the reduction reaction according to Eq. (6).

$$Ar{-}CH{=}N{-}Ar + 4e^- + 4H^+ \longrightarrow Ar{-}CH_3 + H_2N{-}Ar \qquad (6)$$

For the metal complexes **1**, **2**, **3**, and **5** the DC polarogram of each comprises two waves, the first one is due to the reduction of the azomethine center, whereas the more negative one represents the reduction of the metal ion. The relative wave heights of these waves is 2:1 denoting that the number of electrons involved in the wave of the azomethine center is almost double as that of the metal ions. Since the reduction of the metal ion involves two electrons, then the reduction of the azomethine group involves four electrons.

Analysis of the waves due to the reduction of the metal ions and the ligand revealed that the electrode reaction proceeds in an irreversible manner. The most probable α and n_a values are given in Table 7.

It is worthy to mention that the bonding of metal ions to the ligand causes an obvious shift of $E_{1/2}$ of the azomethine wave to more negative potentials. This can be explained on the basis that the bonding of the metal ions to the ligand, which takes place through proton displacement from the OH group, is more ionic than for hydrogen ions. This increases the denoting character of the substituents which in turn increases the charge migration to the CH=N group, hence the aquisitation of the electrons by the azomethine group would require a higher energy.

The CV curve for the ligand exhibits one cathodic peak at $E_p = 1.24$ V but no obvious anodic peaks. This behaviour is in favour of the 4 electron reduction of the azomethine group since the 2 electron process leading to the hydrazo stage must display an anodic peak [37]. For the metal complexes, the CV curves display two cathodic peaks, the less negative one represents the reduction of the azomethine group whereas the more negative one is due to the reduction of the metal ions (Fig. 4).

The peak potentials E_p shift to more negative values on increasing the scan rate which denotes the irreversible nature of the electrode reactions [38]. The plot of E_p as a function of $v^{1/2}$ (scan rate) is a linear relation with positive slope supporting

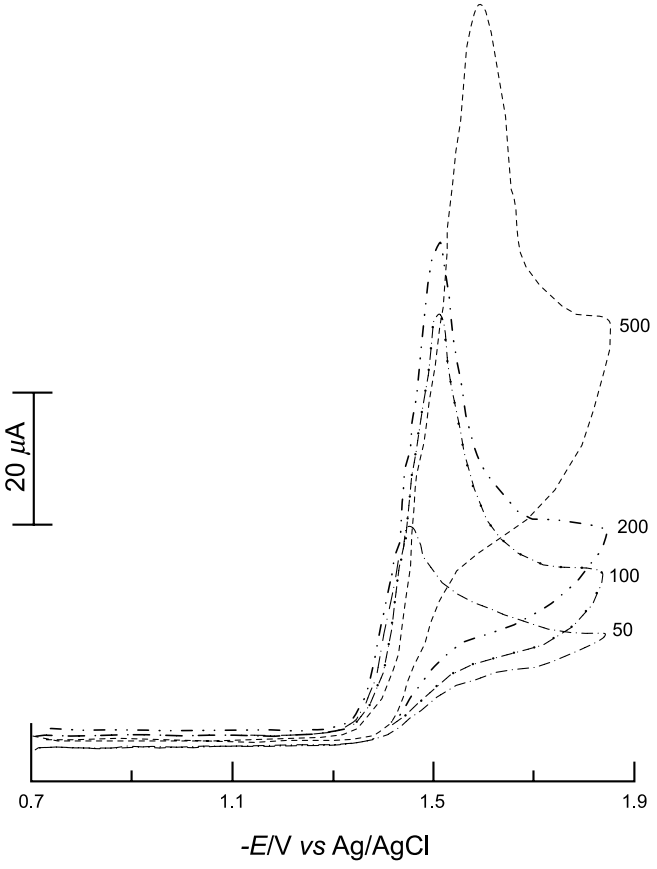

Fig. 4. Cyclic voltammograms of complex **1** at different scan rates

the irreversible electrode process. Further support for the irreversible reactions is gathered from the absence of anodic peaks. Also the i_p *vs*. v plot, is a linear relation with positive slope denoting that the electrode reaction is mainly governed by diffusion. The data are collected in Table 7.

Biological Effects

A primary study of the Minimum Inhibitor Concentrations (*MIC*) of *Schiff* base and its complexes on *Gram* positive bacteria (*Staphylococcus aureus* and *Bacillus subtilis*) and *Gram* negative bacteria (*Escherichia coli* and *Pseudo-monos aeruginosa*) are recorded in Table 8.

From Table 8, it is clear that the inhibition is much larger for most metal complexes than the *Schiff* base on *Gram* positive and *Gram* negative bacteria. The Cu(II) complexes **5** and **6** have the best inhibitor effect on *Gram* negative and *Gram* positive bacteria compared to the other metal complexes. The binuclear Ni(II) complex **4** has also an inhibitor effect on both *Gram* positive and *Gram* negative bacteria but it is less effective than complex **5** on Staphylococcus aureus. The antibiotic effect of binuclear Cu(II) complex **6** on *Gram* negative and *Gram* positive bacteria is relatively stronger than that of complex **5**. As gathered from

Table 8. Minimum inhibitor concentration of *Schiff* base and complexes against *Gram* negative and *Gram* positive bacteria

Organism	Bacteria			
	Gram negative		*Gram* positive	
Compound	*E coli*	*Ps aur*	*B sub*	*St aur*
Ligand	250	150	100	250
Complex **2**	100	100	3.1	100
Complex **3**	50	100	100	50
Complex **4**	50	3.1	100	50
Complex **5**	3.1	50	100	3.1
Complex **6**	50	3.1	3.1	50

data given in Table 8, the order of inhibition of all complexes in the activity of the bacteria studied can be arranged as follows. For Escherichia coli **5** > **3**, **4**, **6** > **2** > ligand, for Pseudomonos aeruginosa **4**, **6** > **5** > **2**, **3** > ligand, for Bacillus subtilis **2**, **6** > **3**, **4**, **5**, ligand, and for Staphylococcus aureus **5** > **3**, **4**, **6** > **2** > ligand.

Such increased activity of the metal chelates can be explained on the basis of chelation theory [39]. On chelation, the polarity of the metal ion will be reduced to a great extent due to the overlap with the ligand orbital. Further, it increases the

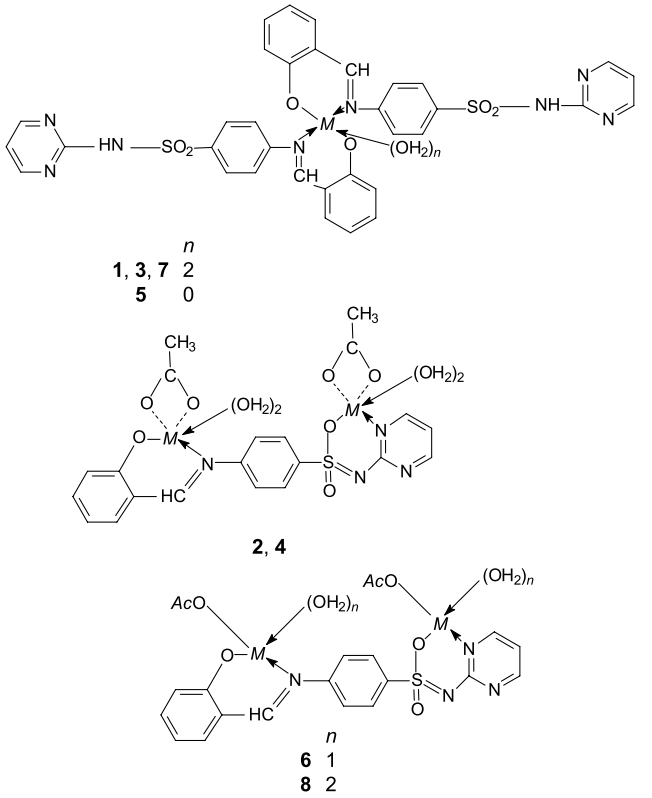

Scheme 3

delocalisation of π-electrons over the whole chelate ring and enhances the lipophilicity of the complexes [40].

Based on the information gained in the present study, the bonding of the metal ions to the ligand can be represented as shown in Scheme 3.

Experimental

Physical Measurements

All reagents were of the highest grade available from BDH and used without further purification. The equipments and the methods employed in the present work were the same as reported earlier [41, 42].

Elemental analysis (C, H, N) was done at the micro analytical laboratory of Cairo University. IR spectra were recorded on a Perkin Elmer 1430 spectrometer as KBr discs. Electronic spectra were registered on a Shimadzu 240 UV-Vis spectrophotometer using Nujol mull technique. Magnetic susceptibility measurements at room temperature (25°C) were determined on a Johnson Matthey magnetic susceptibility balance using $Hg[(Co(SCN)_4]$ as calibrant; diamagnetic corrections were calculated from *Pascal*'s constants. Conductance measurements were carried out by means of a YSI model 32 conductance meter in *DMF* (10^{-3} *M*). The thermal studies, TGA and DTA, were achieved using a Shimadzu TG 5O thermal analyzer. The ESR spectra were recorded on a Joel model JES FE_2 XG spectrometer provided with an E 101 microwave bridge.

The pen recording polarograph Sargent-Welch model 4001 was used for studying the polarographic behavior of the complexes under investigation. The cell described by *Meites* [43] was used for recording the polargramms at a dropping mercury electrode (DME) ($m = 1.03\,\mathrm{mgs}^{-1}$, $t = 3.3$ s at mercury height $h = 60$ cm) and a saturated calome electrode (SCE) as a reference electrode, supplied by Sargent-Welch.

The cyclic voltammogramms of the complexes under investigation were recorded using a potentiostate model 264 A (PAR-from EG&G). The 303 A electrode assembly, supplied by EG&G, with a hanging mercury drop electrode (area $= 2.6 \times 10^{-2}\,\mathrm{cm}^2$) as a working electrode, a Pt wire as a counter electrode, and $Ag/AgCl/KCl_s$ as reference electrode.

The nutrient agar solid medium contained per $1000\,\mathrm{cm}^3$ ($pH = 7.2$): beef extract 3 g, peptone 5 g, Nail 5 g, and agar 20 g. It was sterilized under high pressure steam for 30 min, serial dilutions of the *Schiff* base and its complexes were prepared containing $250\,\mu\mathrm{g/cm}^3$ down to $3\,\mu\mathrm{g/cm}^3$. The bacteria used for testing the biological activity of the ligands and their complexes were *Gram* positive bacteria (Staphylococcus aures and Bacillus subtilis) and *Gram* negative bacteria (Escherichia coli and Pseudomonos aeruginosa) provided by the biology department. The bacteria chosen were found to be sensitive towards metal complexes.

Preparation of Schiff Base

The *Schiff* base was prepared by refluxing a mixture of an ethanol solution of sulfadiazine (1 mmol in $30\,\mathrm{cm}^3$) and an ethanol solution of salicylaldehyde (1 mmol in $20\,\mathrm{cm}^3$) for 3 h. On cooling the reaction mixture, the product formed was filtered off, recrystallized from ethanol, washed with diethyl ether, and dried in a vacuum desiccator over silica gel.

Preparation of Complexes

The metal complexes of the sulfadiazine *Schiff* base with Co(II), Ni(II), Cu(II), and Mn(II) ions were prepared by chemical and electrochemical techniques. In the chemical methods, the metal complexes were prepared by refluxing ethanolic solutions of both the *Schiff* base (1 mmol in $30\,\mathrm{cm}^3$) and each of

the metal acetates (2 mmol in 20 cm^3) and sodium acetate solution (0.5 g in 5 cm^3) as buffering agent for 3 h. After cooling the reaction mixture, the separated solids were filtered off, washed with ethanol and diethyl ether and dried over silica gel. The analytical data and physical measurements are listed in Table 1.

The electrochemical technique used was essentially the same as reported previously [44, 45] in which the respective pure metal was used as the anode and Pt as the cathode and the electrolyte was the *Schiff* base (1.9 mmol), dissolved in a mixture of acetone (20 cm^3) and ethanol (20 cm^3) containing 25 mg of Et_4NClO_4.

The anodic dissolution of the metal (Co, Ni, Cu, or Mn) in the electrolyte amounted to 58–64 mg within 2.5–5 h electrolysis at 10 V and 20 mA. The solid complexes formed were collected, washed successively with acetone, ethanol, and diethyl ether, and then dried in a vacuum desiccator.

References

[1] Johnson DK, Murphy TB, Rose NJ, Goodwin WH (1982) Inorg Chim Acta **67**: 159
[2] Hao Y, Shen H (2000) Spectrochimica Acta (A) **56**: 1013
[3] Tantaru G, Dorneau V, Stan M (2002) J Pharm Biomed Anal **27**: 827
[4] Srinivasan K, Perrier S, Kochi G (1986) J Mol Cat **36**: 297
[5] Jeewoth T, Li Kam Wah H, Bhowon MG, Ghoorohoo D, Babooram K (2000) Synth React Inorg Met Org Chem **30**: 1023
[6] Boghaei DM, Sabounchei SJS, Rayati S (2000) Synth React Inorg Met Org Chem **30**: 1535
[7] Wu S, Lu S (2003) J Mol Cat (A) **197**: 51 and references therein
[8] Kwiatkowski E, Romanowski G, Nowicki W, Kwiatkowski M, Suwinska K (2003) Polyhedron **22**: 1009
[9] Maki T, Hashimato H (1952) Bull Chem Sec Jpn **25**: 41127
[10] Papie S, Kaprivanae N, Grabarie Z, Paracosterman D (1994) Dyes Pigments **25**: 229
[11] Ganolkar MC (1985) Nat Acad Sci **8**: 343
[12] Bergant F, Pacor S, Ghosh S, Chattopadhyay SK, Sava G (1993) Anti Cancer Res **13**: 1007
[13] Raman N, Kulandai Samy A, Thangaraja C, Jeysubramanian K (2003) Trans Met Chem **28**: 29
[14] Elmorsi MA, Gaber M (1996) J Chim Phys (France) **93**: 1556
[15] Torre MH, Facchin G, Kremer E, Castollano EE, Piro OE, Baran EJ (2003) J Inorg Biochem **94**: 200 and references therein
[16] Jayabalakrishnan C, Natarajan K (2002) Trans Met Chem **27**: 75
[17] Geary WJ (1971) Coord Chem Rev **7**: 81
[18] Coats AW, Redfern JP (1964) Nature **68**: 202
[19] Tumer M, Koksal H, Sener MK, Serin S (1999) Trans Met Chem **24**: 414
[20] Deacon GB, Phillips RJ (1980) Coord Chem Rev **33**: 227
[21] Nakamoto K (1963) Infrared Spectra of Inorganic and Coordination Compounds. Wiley Interscience, New York, pp 197–201
[22] Nakamoto K (1963) Infrared Spectra of Inorganic and Coordination Compounds. Wiley Interscience, New York, pp 81–83
[23] Zaki ZM, Mohamed GG (2000) Spectrochimica Acta(A) **56**: 1245
[24] El-Sonbati AZ, El-Bindary AA, Mabrouk EM, Ahmed RM (2001) Spectrochemica Acta(A) **57**: 1751
[25] Rao CNR (1976) Chemical Applications of IR spectroscopy. Academic Press, New York, p 258
[26] Kondo M, Kuob N (1958) J Phys Chem **62**: 1558
[27] Lever ABP (1968) Inorganic Electronic Spectroscopy. Elsevier, Amsterdam, p 341
[28] Figgs BN, Lewis J (1967) Modern Coordination Chemistry. Interscience, New York
[29] Konig E (1971) Structure Bonding (Berlin) **9**: 175

[30] Figgis BN (1976) Introduction to Ligand Fields. Wiley Eastern, p 316
[31] Lever ABP (1968) Inorganic Electronic Spectroscopy. Elsevier, Amsterdam
[32] Chandra S, Sharma SD (2002) Trans Met Chem **27**: 732
[33] Von Telewsky A, Fievz H (1973) Adv Chim Acta **56**: 977
[34] Drago RS (1977) Physical Methods in Chemistry. Saunders, Philadelphia
[35] Fidone SI, Stevens KWH (1959) Proc Phys Soc **73**: 116
[36] Zuman P (1969) The Elucidation of Organic Electrode Process. Academic Press, p 28
[37] Sivakumara A, Reddy S, Krishnan V (1983) Indian J Chem **22**(A): 800
[38] Delahay P (1966) New Instrumental Methods in Electrochemistry, chap 6. Interscience, New York
[39] Srivastava RS (1981) Inorg Chim Acta **56**: 65
[40] Gupta N, Swaroop R, Singh RV (1997) Main Group Met Chem **14**: 387
[41] Gaber M, El-Baradie KY, Amer SA, Issa RM (1991) Synth React Inorg Met Org Chem **21**: 349
[42] Gaber M, El-Baradie KY, Issa RM, El-Mehassab IM (1992) Synth React Inorg Met Org Chem **22**: 1097
[43] Meites L (1965) Polarographic Techniques. Interscience, New York, p 240
[44] Mabrouk HE, Tuck DG (1988) Inorg Chim Acta **145**: 237
[45] Mabrouk HE, Gaber M, El-Sonbati AZ, El-Hefnawey GB (1992) Trans Met Chem **17**: 1